RSC Advances

ROYAL SOCIETY OF CHEMISTRY

www.rsc.org/advances

Structural and Magnetic Properties of Ferrihydrite Nanoparticles

C.J. Masina*[1], J.H. Neethling[1], E.J. Olivier[1], S. Manzini[2], L. Lodya[2], V. Srot[3], and P.A. van Aken[3]

[1]Centre for HRTEM, Nelson Mandela Metropolitan University, PO Box 77000, Port Elizabeth, South Africa
[2]Sasol Technology, R&D, 1 Klasie Havenga Road, Sasolburg, South Africa
[3]Stuttgart Center for Electron Microscopy, Max Planck Institute for Intelligent Systems, Heisenbergstr. 3, 70569
Stuttgart, Germany

Abstract: Ferrihydrite is a short range ordered iron (III) oxyhydroxide that has been recently recognized as a good catalyst for Fischer-Tropsch synthesis of liquid hydrocarbons. Despite the critical role of ferrihydrite in many disciplines, its mineral structure remains a topic of debate. The main aspect of its structure which has been debated is the presence or absence of tetrahedrally coordinated Fe^{3+} in its mineral structure. In this work, electron energy-loss spectroscopy (EELS) was used to probe the Fe $L_{2,3}$ edges of ferrihydrite and reference spectra of different iron oxide compounds and the percentage of Fe^{3+} in T_d symmetry was estimated from non-linear least squares (NLLS) fitting coefficients. EELS results demonstrate that Fe^{3+} in T_d coordination is present in substantial amounts in the structure of ferrihydrite. These findings were supported by Mössbauer spectroscopy results performed on the same ferrihydrite samples.

1. Introduction

For almost two decades the crystal structure of ferrihydrite (Fh) has been described by a three-component structural model proposed by Drits *et al.*[1] based on a fitted X-ray diffraction pattern; however the contribution from inelastic scattering and other forms of diffuse scattering was ignored. This multiphase model caters for three components: defect-free Fh (f-phase), defective Fh (d-phase), and ultradispersed hematite, all of which have Fe^{3+} cations in octahedral coordination. Michel and co-workers[2] performed pair distribution function (PDF) analyses of high energy synchrotron data of Fh nanoparticles which did not match the PDFs calculated from Drits three-component model. Instead, they proposed a new "single" phase structural model (hexagonal space group $P6_3mc$ with lattice parameters a = 5.95 Å and c = 9.06 Å) which successfully reproduced the experimental PDFs of Fh and in which iron atoms occupy three distinct symmetry sites: Fe1, Fe2, and Fe3. The Fe1 and Fe2

---

[*] Corresponding author: colani.masina@nmmu.ac.za

sites are both octahedrally coordinated, however they occupy a different Wyckoff position with slightly differing Fe-O geometries; the central Fe3 is tetrahedrally coordinated. Each oxygen ion in the tetrahedron is linked to three edge-shared Fe octahedra. The Fe1 sites arranged itself in an edge-sharing layers separated by a mixed layer of Fe2 and Fe3 sites. In its ideal form this model predicts iron site occupancy of 80% for the octahedral sites (Fe1 and Fe2) and 20% for the tetrahedral sites (Fe3).[2]

Michel's model was criticized by different groups, for example some authors objected to the use of a periodic model to describe the positions of atoms in the limited number of unit cells in a nanocrystalline material like Fh.[3, 4] It also failed to reproduce the experimental XRD pattern of Fh, high measured density, and violating Pauling's bond valence sum rule (Pauling 2nd rule), because some ^{IV}Fe-O distances are equal or larger than the ^{VI}Fe-O distances.[3] A slightly revised model was proposed by Michel and co-workers[5] which successfully addressed the concerns about violation of the Pauling 2nd rule and explained the discrepancies between measured and calculated densities as a result of the difference in the cationic occupancies in the structure of Fh. Both the original and revised models share the same akdalaite polyhedra structure[6] with the 13 Fe units where the central tetrahedral coordinated iron (Fe3) is connected to 12 peripheral octahedral iron (Fe1 and Fe2) via μ_4-oxo bridges[7] in an edge sharing array.

One of the controversies regarding the structure of Fh lies in the presence or absence of tetrahedrally (Td) coordinated Fe^{3+} within its structure. The local electronic structure at the Fe sites in iron oxide systems has been extensively investigated by electron energy loss spectroscopy (EELS)[8-21] using the Fe L-edge which is conventionally characterized by two intense sharp peaks termed "white lines". These two peaks result from excitations from initial states $2p^6 3d^n$ to $2p^5 3d^{n+1}$ final states and the edge splits to L_3 and L_2 lines due to the dipole selection rule $\Delta l = \pm 1$.[22, 23] In addition, crystal field causes the splitting of the degenerated $3d$ orbitals to $e_g + t_{2g}$ and $t_2 + e$ for octahedral and tetrahedral symmetry, respectively.[22, 24] These fine structure features introduced by crystal field splitting of the $L_{2,3}$ edges are highly specific to the Fe site symmetry.[25] Based on estimation by linear extrapolation to very low electron dose (1 electron nm^{-2}), Pan *et al.*[14, 16, 26] ruled out the presence of T_d Fe^{3+} in pristine Fh and suggested that T_d Fe^{3+} could have been introduced by electron beam damage. It was however emphasised that the exact intrinsic structure of the nanocrystalline Fh still remains unclear, since their extrapolation extended to extremely low electron dose (1 electron nm^{-2})

that is practically impossible to achieve.[16] It is also worth mentioning that fitting the spectrum recorded at the lowest possible dose achieved by these authors (3×10^4 electron nm^{-2}), without the extrapolation, yielded a significant amount (25 ±5 %) of iron in tetrahedral coordination.[26] Most recently, Peak and Regier[25] probed the Fe $L_{2,3}$ edges of 2LFh using synchrotron based X-ray absorption spectroscopy (XANES), and their study supported the presence of T_d Fe^{3+} within the structure of 2LFh. The relative percentages of octahedrally coordinated (O_h) and T_d Fe^{3+} were obtained by fitting the experimental inverse partial fluorescence yield (IPFY) data of γ-Fe_2O_3 and 2LFh with theoretical calculated data. A significant amount (30-40 %) of T_d Fe^{3+} in the 2LFh structure was produced as the result of the fitting. The similarities of IPFYs between γ-Fe_2O_3 and 2LFh provided further evidence of the presence T_d Fe^{3+} in 2LFh.[27] Iron $L_{2,3}$ X-ray magnetic circular dichroism (XMCD) measurements by Guyodo *et al.*[28] also suggested a concentration of 20-30 % tetrahedral sites in the structure of Fh.

In this study the structural and magnetic properties of nanoparticles of 2-line Fh and 6-line Fh synthesised using rapid hydrolysis of $Fe(NO_3)_3x9H_2O$ solutions are investigated. It forms part of a comprehensive investigation aimed at understanding the thermal transformation and reduction behaviour of Fh as well as the role of SiO_2 as structural promoter/binder on the reduction mechanism. The focus of this work is to provide detailed understanding of the Fe^{3+} coordination environment in the crystal structure of Fh, an important iron-based catalyst for Fischer-Tropsch synthesis.[29] The investigation methods include EELS, low and room temperature Mössbauer spectroscopy.

2 Experimental Procedures

Sample description

Two samples, namely 2-line Fh (labelled 2LFh) and 6-line Fh (labelled 6LFh) synthesised by using rapid hydrolysis of $Fe(NO_3)_3{\cdot}9H_2O$ solutions are investigated. 2LFh nanoparticles were synthesized by rapid hydrolysis of $Fe(NO_3)_3.9H_2O$ in a water solution, a method previously reported by Schwertmann Cornell[30] and 6LFh nano-crystalline particles were prepared using a method described by Carta.[31] The details of the synthesis route are described in ref.[32] Nanoparticles of 2LFh were found to be of poor crystallinity with average crystallite size of ~ 4.0, while 6LFh was found to be of a relatively better crystallinity with an average crystallite size of ~ 6.0 nm. [32]

EELS Experiments

EELS measurements were performed using the Zeiss Sub-Electron-Volt-Sub-Angstrom-Microscope (SESAM) transmission electron microscope (Zeiss, Oberkochen) operated at 200 kV and equipped with an electrostatic Ω-type monochromator and MANDOLINE filter. Full description and capabilities of the SESAM microscope are described elsewhere.[33, 34] Samples for EELS measurements were prepared by grinding Fh powder with a mortar and pestle and ultrasonicating the powder in ethanol to disperse particles, and a drop of the suspension in ethanol was deposited on lacey carbon TEM grid.

EELS spectra obtained in image mode were acquired with an energy resolution of about 0.2 eV at an energy dispersion of 0.037 eV/channel using a collection angle of 3 mrad. In all samples four different areas were investigated and at each position 100 spectra were acquired. Afterwards, all spectra were aligned and averaged using a script developed at StEM (MPI-IS, Stuttgart, Germany) for Digital Micrograph. The local Fe symmetry in 2LFh and 6LFh, particularly the possible existence of Td Fe^{3+} within their structures was investigated using reference spectra of hematite (α-Fe_2O_3: O_h Fe^{3+}); maghemite (γ-Fe_2O_3: 62.5 % O_h Fe^{3+} and 37.5 % T_d Fe^{3+}); magnetite (Fe_3O_4: O_h Fe^{3+}/Fe^{2+} and T_d Fe^{3+}); and wüstite (FeO: O_h Fe^{2+}). Prior to fitting, spectra were processed using Gatan's Digital Micrograph (DM) software (Gatan Microscopy Suite 2.11.1404.0). The energy scales were calibrated using energy values reported by van Aken *et al.*.[19, 20] For Fe^{3+} bearing α-Fe_2O_3 and γ-Fe_2O_3, the main peak was set at 709.5 eV and for Fe^{2+} compound (FeO) it was set at 707.8 eV. For mixed valence compound Fe_3O_4 the maximum of the L_3 edge was centered at 708.9 eV. The spectra were then background subtracted using the power law model.[35] To obtain a single scattering distribution (SSD), plural scattering was removed by the Fourier-ratio deconvolution method[35] using low-loss spectra taken at the same experimental conditions as the Fe $L_{2,3}$ edge.

A non-linear least squares (NLLS) fitting routine performed within IGOR Pro (version 6.32A) software previously reported by Pan *et al.*[15, 16] was adapted in this work. This software was preferred over MLLS/NLLS fitting performed in DM, because it provides the user with options to constrain the fitting coefficients and accommodate small energy shift in edge positions.[16] In all the procedures, the fitting parameters were constrained in that the coefficients of each reference spectrum were set to be greater than zero and small energy shifts were allowed to occur (-0.3 to 0.3 eV) during fit iterations according to the approach proposed by Pan *et al.*[16]

Mössbauer spectroscopy measurements

Mössbauer spectroscopy (MS) measurements were performed at room temperature (RT) using a conventional acceleration constant spectrometer operating in the absorption mode and equipped with a ^{57}Co/Rh source. Low temperature (LT) and applied magnetic field measurements were performed using the Spectromag SM4000-10 cryomagnet from Oxford Instruments designed to operate at variable temperatures (1.3 – 300 K) and applied magnetic fields up to 10 T. The MS spectra were analyzed by means of a least squares program "Normos" that models them using six-line (sextet) subspectra based on a Lorentzian line-shape profile. The individual absorption features were then identified on the basis of the corresponding hyperfine parameters, i.e. the isomer shift (δ), quadrupole splitting (ΔE_Q) and magnetic hyperfine field (B_{hf}) values. The relative content of each phase was determined from the area (A) of the absorption peaks. Metallic iron (α-Fe) is used to calibrate the velocity scale of the MS spectra, i.e. the isomer shift values of all the species are reported relative to it.

3 Results and Discussion

Electron Energy Loss Spectroscopy

Iron in minerals exists commonly in Fe^{2+} and Fe^{3+} oxidation states which are mostly octahedrally (O_h) coordinated; tetrahedral (T_d) coordination is however also possible. The background-corrected Fe $L_{2,3}$ edges of 2LFh and 6LFh are compared in Figure 1 to spectra acquired from reference compounds containing Fe^{3+} and/or Fe^{2+} which are used in the fitting procedures.

All the Fe $L_{2,3}$ edges in Figure 1 are characterized by sharp maxima referred to as "white lines" [12, 13] and all structural features present in the EELS spectra are similar to those previously identified by Chen and co-workers.[9] Hematite (α-Fe_2O_3) shows a characteristic Fe L_3 edge with an intense pre-peak at ~ 708.0 eV leading to the main Fe L_3 peak at 709.5 eV.[20]

The large Fe L_3 splitting feature in α-Fe_2O_3 was attributed to the strong ligand-field splitting from O_h symmetry around the Fe^{3+} ion.[9] Maghemite (γ-Fe_2O_3) also shows features of Fe^{3+} with an Fe L_3 pre-peak which is less intense as compared to α-Fe_2O_3.

It is well known that the crystal-field splitting is affected by factors such as the type of ligand and the geometry of the complex[24] and that the ligands in γ-Fe_2O_3 form O_h and T_d symmetry.[36] The contribution of complexes coordinated in T_d geometry to the crystal-field splitting is less compared to octahedral crystal fields due to fewer ligands in T_d symmetry.[24] As a result, γ-Fe_2O_3 does not show a strong splitting as compared to α-Fe_2O_3. Wüstite (FeO), the Fe^{2+} bearing compounds, shows a ~ 2 eV chemical shift to lower energy with respect to the Fe^{3+} compounds.[9]

Usually iron oxy-hydroxides show a significantly weaker splitting of the Fe L_3 peak as compared to α-Fe_2O_3 due to the weak crystal field around the iron atoms.[9] Apart from oxygen ligands, other factors that contribute to the weak ligand field in the Fh molecular orbitals are the presence of weak-field ligands ((OH/H_2O) which are expected to produce small crystal-field splitting and the poor crystallinity[9] as well as the possible presence of ligands in T_d symmetry.[2, 25, 28, 37]

Figure 1: Fe $L_{2,3}$ edges of 2LFh, 6LFh and different Fe oxide reference materials. The Fe $L_{2,3}$ spectra are vertically shifted for clarity.

Figure 2 shows the EELS spectra of 2LFh fitted only with Fe^{3+} references. The fitting was restricted to the Fe L_3 edge covering an energy range from 702 to 718 eV in order to be consistent with fitting procedures reported in literature.[16, 20] The fitting coefficients are given in Table 1 together with those for 6LFh. The fit in Figure 1: Fe $L_{2,3}$ edges of 2LFh, 6LFh and different Fe oxide reference materials. The Fe $L_{2,3}$ spectra are vertically shifted for clarity.

Figure 2 is rather poor where a mismatch on the low energy side of the peak (shown by an arrow) is obvious.

Figure 1: Fe $L_{2,3}$ edges of 2LFh, 6LFh and different Fe oxide reference materials. The Fe $L_{2,3}$ spectra are vertically shifted for clarity.

Figure 2: NLLS fit of 2LFh showing the mismatch at the lower energy side of the main Fe *L*3 peak. The spectrum was fitted with a hematite and maghemite reference spectra. The difference spectrum is plotted on the same scale, however shifted vertically for clarification.

Figure 3 shows the EELS spectra of 2LFh and those of three reference materials that produced the best fit which include a Fe L_3 reference spectra for Fe^{3+} and Fe^{2+}. The presence of the Fe^{2+} species is most likely a result of electron beam damage, enhanced by the fact that the specimen was not cooled during TEM investigations. It is known that the iron in Fh only exists in trivalent state [30, 36] and this has been validated by MS measurements in this work. MS is considered to be a more reliable technique than electron microscopy which is known to cause electron beam-induced reduction in the material.[14] It has been previously suggested that electron beam-induced damage in iron hydroxides occurs via the loss of the iron coordinating ligands such as O, OH, and H_2O induced by hydrolysis. This process results in the structural rearrangement and reduction of the iron within the iron hydroxide coordination complex.[14, 16] Pan *et al.*,[14] estimated that Fe^{2+} is produced in synthetic 6LFh when the electron dose exceeds 10^8 electrons /nm^2 and it is therefore reasonable to assume that the Fe^{2+} observed in the current 2LFh specimens could be due to electron beam reduction of Fe^{3+}.

Besides the fact that iron in Fe^{2+} state was required to obtain a satisfactory fit, the features in our Fe *L*-edge EELS spectra of synthetic Fh still look very similar to the spectra reported by Gloter *et al.*[11] and Chen *et al.*.[9] As a result, we maintain that our EELS Fe L_3 edge contains enough information to evaluate the presence or absence of tetrahedrally coordinated Fe^{3+} in Fh. Following EELS fitting procedures of Fh *L*-edge reported by Pan and co-workers[26], the percentage of O_h and T_d Fe^{3+} from our EELS data were estimated from the weighting coefficients of each reference spectra. The best NLLS fit for the Fe L_3 edge of 2LFh is obtained by using a model function consisting of α-Fe_2O_3, γ-Fe_2O_3 and FeO references with the relative proportions of 37, 56 and 7%, respectively (see Table 1). Our NLLS fitting results suggest that a significant portion of Fe^{3+} in 2LFh is in tetrahedral coordination with an estimated amount of 20 ± 6 %. This result is consistent with EELS measurements taken at the lowest electron fluence of ~10^5 electron/nm^2 which suggests that as much as 25 % of Fe^{3+} is present in tetrahedral coordination.[26] However, based on extrapolation of the same data to very low fluence (1 electron/nm^2), the authors found that the O_h Fe^{3+} content could be extrapolated up to 100 % and they concluded that the T_d Fe^{3+} could be absent in the pristine structure of Fh and that its presence was only a result of electron beam damage.[26]

Figure 1: Fe $L_{2,3}$ edges of 2LFh, 6LFh and different Fe oxide reference materials. The Fe $L_{2,3}$ spectra are vertically shifted for clarity.

Figure 2: NLLS fit of 2LFh showing the mismatch at the lower energy side of the main Fe $L3$ peak. The spectrum was fitted with a hematite and maghemite reference spectra. The difference spectrum is plotted on the same scale, however shifted vertically for clarification.

Figure 3: EELS spectrum of 2LFh spectrum (black) and calculated fit curve (red), and the relative content of reference materials that produced the best NLLS fit. The difference spectrum is plotted on the same scale, however shifted vertically for clarification.

Figure 4 shows the EELS spectra of 6LFh and reference materials featuring the Fe L_3 edge and the corresponding relative percentages of each reference spectra. As for 2LFh, attempts to fit a model function consisting of a combination of only Fe^{3+} reference spectra to the experimental Fe L_3 edge of 6LFh produced mismatches especially on the low energy side of the Fe L_3 white line (fit not shown). The best NLLS fit for 6LFh was also obtained by a model function consisting of a linear combination of γ-Fe_2O_3, α-Fe_2O_3, and FeO reference Fe L_3 spectra with relative abundance of 46, 50 and 4%, respectively. The addition of FeO greatly improved the fit as shown by the improvement in χ^2, where χ^2 is described by[16]

$$\chi^2 = \sum_i \left(\frac{y-y_i}{\sigma_i}\right) \quad (1),$$

where y_i and y are the measured data value and fitted value for a given point, respectively, and σ_i is the standard deviation estimate for y_i.

The percentage of T_d Fe^{3+} as estimated from the NLLS fits amounts to 18 ± 5 %; a value close to previously reported values range 20 – 30% for 6-line Fh.[25, 28, 37] Noteworthy, the amount of Fe^{3+} in O_h and T_d coordination obtained from NLLS fittings represent the percentage of O_h and T_d coordination and not the fitted fraction of each reference spectrum.[38]

It appears as if the minor occurrence of the Fe^{2+} was 'localized' and it did not alter the Fe L-edge main spectral features since there is still consistency between Fe L-edge XANES[25], EELS[9, 11] and results presented here. It can be seen from Figure 1 that the spectral features of both 2LFh and 6LFh matched that of maghemite more closely than that of hematite. In the hematite spectrum the L_3 peak split is well pronounced and well resolved, which is an indication of the presence of only one Fe^{3+} site, i.e. octahedral,[25] and for maghemite, the splitting of L_3 peak was well resolved (Fig.1). Our results are in good agreement with the Fe *L*-edge XANES results of Peak and Regier.[25] The L_3 spectral blurring observed for maghemite was previously attributed to the presence of both distorted O_h and T_d Fe^{3+} sites.[39] Consequently, similarities between 2LFh and maghemite were used to validate the presence of T_d Fe^{3+} in the Fh structure by Peak and Regier.[25] However, this was disputed by Manceau[40] stating that the blurring in the Fh L_3 peak can be explained by the disordered nature of Fh and not the presence of tetrahedrally coordinated Fe^{3+} and the similarities between maghemite and 2LFh L_3 features were labeled as a coincidence. A subsequent discussion by Peak and Regier[41] indicated that it was unlikely that the disordered nature of Fh alone caused the broadening observed in the L_3 peak since even a highly disordered akaganeite showed a well resolved L_3 peak (see Fig. 2 in ref.[25]). This lead Peak and Regier[25] to conclude that the similar features observed in maghemite and Fh *L*-edge spectra indeed result from the presence of T_d Fe^{3+} sites in the structure of the material. With respect to the Fe^{3+} coordination environment in Fh, our EELS results support the findings of Peak and Regier.[25] This conclusion was based firstly on the similarities of maghemite and Fh spectral features, and secondly on the satisfactory fits obtained when Fh was modeled with standard spectra consisting mainly of maghemite.

Mössbauer Spectroscopy

As mentioned earlier, Mössbauer spectroscopy (MS) measurements were performed at 4.2 K in zero applied magnetic field (ZFMS) and at 4.2 K in an external magnetic field (B_{app}) of 10 T applied parallel to the direction of γ-rays, referred to as in field Mössbauer spectroscopy (IFMS). Note the internal hyperfine magnetic field (B_{hf}) obtained in ZFMS and the effective magnetic field (B_{eff}) measured in IFMS are related according to equation (2)[42]

$$\vec{B}_{eff} = \vec{B}_{app} + \vec{B}_{hf} \qquad (2).$$

The direction of $\vec{B}_{hf}$ is usually taken to be opposite to that of the magnetisation ($\vec{M}$) and, in practice, the alignment of the spins is never perfect such that the relation between B_{eff} and B_{hf} is given by equation (3)[43]

$$B_{hf}^2 = B_{eff}^2 + B_{app}^2 - 2\,B_{eff}B_{app}\cos\theta \qquad (3),$$

where θ is the angle between B_{app} and M. When the direction of the applied field is parallel to the direction of γ-rays, B_{eff} values and the intensities of the lines of a MS spectrum change as follows: For ferromagnetic (FM) materials $B_{eff} \approx B_{hf} - B_{app}$ and the ratios of intensities of the lines of the MS spectrum[†] amount to 3:0:1:1:0:3, i.e. the lines 2 and 5 cancel out. For ferrimagnetic (FiM) materials, $B_{eff} \approx B_{hf} - B_{app}$ and the intensities of the lines 2 and 5 cancel out on the B sites while $B_{eff} \approx B_{hf} + B_{app}$ and the intensities of the lines 2 and 5 cancel out on the A sites. For antiferromagnetic (AFM) materials, $B_{eff} \approx B_{hf}$ and the ratios of the intensities of the lines of the MS spectrum change to 3:4:1:1:4:3.

ZFMS and IFMS measurements have been used extensively in the past as tools to characterise the structure of Fh, but there is still controversy regarding the interpretation of the results in terms of Fe^{3+} coordination.[44-47] Murad[48] suggested that Fe^{3+} is mainly in O_h coordination while a small fraction is in T_d coordination. The presence of T_d Fe^{3+} in the structure of Fh was ruled out by Cardile[49] and by Pankhurst & Pollard[46] based on IFMS results. However, Zhao and co-workers[47] refuted these claims and argued in favour of the presence of T_d Fe^{3+} in Fh. In the present study attempts were made to fit both the ZFMS and IFMS spectra of 2LFh and 6LFh according to the structural model of Fh proposed by Michel *et al.*.[2, 5]

Figure 1: Fe $L_{2,3}$ edges of 2LFh, 6LFh and different Fe oxide reference materials. The Fe $L_{2,3}$ spectra are vertically shifted for clarity.

Figure 2: NLLS fit of 2LFh showing the mismatch at the lower energy side of the main Fe *L*3 peak. The spectrum was fitted with a hematite and maghemite reference spectra. The difference spectrum is plotted on the same scale, however shifted vertically for clarification.

[†] In the absence of an applied magnetic field the lines of a magnetically split MS spectrum are counted 1, 2, 3, 4, 5 and 6 from left to right with relative ratios of 3:2:1:1:2:3 for randomly distributed particles.

Figure 3: EELS spectrum of 2LFh spectrum (black) and calculated fit curve (red), and the relative content of reference materials that produced the best NLLS fit. The difference spectrum is plotted on the same scale, however shifted vertically for clarification.

Figure 4: The EELS spectrum of 6LFh (black) and corresponding best fit curve (red), and the relative proportions of the three reference compounds that produced the best NLLS. The difference spectrum is plotted on the same scale, however shifted vertically for clarification.

Figure 5 shows ZFMS spectra of 2LFh and 6LFh recorded at 4.2 K and Figure 1: Fe $L_{2,3}$ edges of 2LFh, 6LFh and different Fe oxide reference materials. The Fe $L_{2,3}$ spectra are vertically shifted for clarity.

Figure 2: NLLS fit of 2LFh showing the mismatch at the lower energy side of the main Fe *L*3 peak. The spectrum was fitted with a hematite and maghemite reference spectra. The difference spectrum is plotted on the same scale, however shifted vertically for clarification.

Figure 3: EELS spectrum of 2LFh spectrum (black) and calculated fit curve (red), and the relative content of reference materials that produced the best NLLS fit. The difference spectrum is plotted on the same scale, however shifted vertically for clarification.

Figure 4: The EELS spectrum of 6LFh (black) and corresponding best fit curve (red), and the relative proportions of the three reference compounds that produced the best NLLS. The difference spectrum is plotted on the same scale, however shifted vertically for clarification.

Figure 5: Mössbauer spectra recorded at 4.2 K for (a) 2LFh and (b) 6LFh. Fe1, Fe2 and Fe3 correspond to the three types of Fe sites in ferrihydrite structure, i.e. octahedrally (Fe1 and Fe2) and tetrahedrally (Fe3) coordinated sites.

Figure 6 shows the corresponding IFMS spectra at 4.2 K in an applied magnetic field of 10 T. The corresponding hyperfine parameters are given in Table 1: Fitting coefficients for 2LFh and 6LFh from NLLS fitting without and including wüstite in the fitting routine. χ^2 is calculated following equation (1).

Table 2 together with the relative resonance absorption areas for each of the three Fe sites. ZFMS spectrum of 2LFh yields three six-line sub-spectra (sextets) with parameters δ_1 = 0.49 mm/s, ΔE_{Q1} = -0.08 mm/s and B_{hf1} = 49.1T, δ_2 = 0.44 mm/s, ΔE_{Q2} = -0.07 mm/s and B_{hf2} = 45.4 T, and δ_3 = 0.47 mm/s, ΔE_{Q3} = 0.02 mm/s and B_{hf3} = 51.4 T. For 6LFh the ZFMS spectrum gives three sextets with δ_1 = 0.50 mm/s, ΔE_{Q1} = -0.05 mm/s and B_{hf1} = 49.3 T, δ_2 = 0.43 mm/s, ΔE_{Q2} = -0.05 mm/s and B_{hf2} = 45.8 T, and δ_3 = 0.50 mm/s, ΔE_{Q3} = 0.01 mm/s and B_{hf3} = 51.6 T. All these values are within the ranges $\delta \approx 0.45 – 0.50$ mm/s, $\Delta E_Q \approx -0.10 – 0.06$ mm/s and $B_{hf} \approx 45.0 – 50.0$ T reported for Fh at 4.2 K from ZFMS measurements.[50-53]

The hyperfine parameters obtained from IFMS spectra (Figure 1: Fe *L*$_{2,3}$ edges of 2LFh, 6LFh and different Fe oxide reference materials. The Fe *L*$_{2,3}$ spectra are vertically shifted for clarity.

Figure 2: NLLS fit of 2LFh showing the mismatch at the lower energy side of the main Fe *L*3 peak. The spectrum was fitted with a hematite and maghemite reference spectra. The difference spectrum is plotted on the same scale, however shifted vertically for clarification.

Figure 3: EELS spectrum of 2LFh spectrum (black) and calculated fit curve (red), and the relative content of reference materials that produced the best NLLS fit. The difference spectrum is plotted on the same scale, however shifted vertically for clarification.

Figure 4: The EELS spectrum of 6LFh (black) and corresponding best fit curve (red), and the relative proportions of the three reference compounds that produced the best NLLS. The difference spectrum is plotted on the same scale, however shifted vertically for clarification.

Figure 5: Mössbauer spectra recorded at 4.2 K for (a) 2LFh and (b) 6LFh. Fe1, Fe2 and Fe3 correspond to the three types of Fe sites in ferrihydrite structure, i.e. octahedrally (Fe1 and Fe2) and tetrahedrally (Fe3) coordinated sites.

Figure 6) for 2LFh amount to δ_1 = 0.47 mm/s, ΔE_{Q1} = -0.04 mm/s and B_{eff1} = 50.4 T, δ_2 = 0.48 mm/s, ΔE_{Q2} = -0.02 mm/s and B_{eff2} = 43.2 T, and δ_3 = 0.45 mm/s, ΔE_{Q3} = 0.02 mm/s and B_{eff3} = 57.2 T. From IFMS spectra of 6LFh ones obtains δ_1 = 0.48 mm/s, ΔE_{Q1} = -0.04 mm/s and B_{eff1} = 49.7 T, δ_2 = 0.47 mm/s, ΔE_{Q2} = -0.02 mm/s and B_{eff2} = 42.3 T, and δ_3 = 0.47 mm/s, ΔE_{Q3} = 0.02 mm/s and B_{eff3} = 57.1 T for 6LFh. These values are also consistent with $\delta \approx 0.44 - 0.50$ mm/s, $\Delta E_Q \approx -0.08 - 0.04$ mm/s and $B_{eff} \approx 43 - 57$ T as has been reported for Fh from IFMS measurements.[45, 50-53]

The data in Table 1: Fitting coefficients for 2LFh and 6LFh from NLLS fitting without and including wüstite in the fitting routine. χ^2 is calculated following equation (1).

Table 2 show that for both, ZFMS and IFMS measurements, the isomer shift varies in a narrow range $\delta \approx 0.43 - 0.50$ mm/s, typical of Fe^{3+} bearing species. The presence of divalent Fe species as inferred to from EELS analysis of 2LFh and 6LFh is therefore not supported by ZFMS and IFMS results. Indeed, Previous Mössbauer spectroscopy results by Murad *et al*.[45] also showed that iron in natural Fh is only present in Fe^{3+} oxidation state. The narrowness of the δ range observed here for 2LFh and 6LFh seems to imply that the electronic densities around Fe^{3+} nuclei are almost identical. Furthermore, the values of ΔE_Q are small and vary also in a narrow range 0.04 – -0.08 mm/s, which could indicate nearly cubic lattice site symmetry around the Fe^{3+} nuclei.

A comparison between ZFMS and IFMS data (Table 1: Fitting coefficients for 2LFh and 6LFh from NLLS fitting without and including wüstite in the fitting routine. χ^2 is calculated following equation (1).

Table 2) shows that for one of the sextets $B_{eff} \approx B_{hf} \approx 49$ T (and $\Delta E_Q < 0$) and the intensities of the lines 2 and 5 on the IFMS spectra increase as expected for AFM materials.[54] For the second sextet $B_{eff} \approx 43$ T (and $\Delta E_Q < 0$) is slightly smaller than $B_{hf} \approx 45$ T indicating that the spins tend to align antiparallel to B_{app} (i.e. B_{app} tend to subtract from B_{hf}) as usually observed on the octahedral sites of FiM materials.[54] However, contrary to what is expected for FiM materials the intensities of the lines 2 and 5 for IFMS spectra do not cancel out which might indicate that spin alignment is almost completely suppressed due to spin canting and/or to the presence of defects, vacancies and impurities.[55] For the third sextet $B_{eff} \approx 57$ T (and $\Delta E_Q > 0$) is much higher than $B_{hf} \approx 51$ T, i.e. B_{app} adds up to B_{hf}, the intensities of the lines 2 and 5 on IFMS spectra cancel out almost completely; similar behaviour is expected for Fe atoms on the tetrahedral sites of FiM materials.[54] The spin alignment is however also not perfect as indicated by the presence of small residual intensities for the lines 2 and 5.

In summary, the IFMS spectra of both 2LFh and 6LFh are successfully fitted with a model combining an AFM-like sub-lattice and two FiM-like sub-lattices both of which with a certain degree of imperfectly aligned magnetic moments due to spin canting and/or some degree of disorder. This model differs somehow from the two FiM sub-lattices for 2-line Fh and a single AFM sub-lattice for 6-line Fh proposed by Pankhurst and Pollard.[46] It is however compatible with Michel's structural model for Fh; in this scenario the three sextets apparent on the ZFMS and IFMS spectra of 2LFh and 6LFh correspond to the three different Fe sites Fe1, Fe2 and Fe3 of Michel's model. The two sextets with $B_{eff} \approx 49$ T and $B_{eff} \approx 43$ T are ascribed to the octahedrally coordinated Fe1 and Fe2, respectively, while the sextet with $B_{eff} \approx 57$ T is ascribed to the tetrahedrally coordinated Fe3. Both ZFMS and IFMS results give relative abundances of approximately 53% for Fe1 (O_h), 31% for Fe2 (O_h) and 15% for Fe3 (T_d) for 2LFh, and 67% for Fe1 (O_h), 23% for Fe2 (O_h) and 10% for Fe3 (T_d) for 6LFh, respectively. These values are fairly in agreement with the ideal values of 60%, 20% and 20%, respectively, proposed by Michel model.[2, 5]

Usually for Fe^{3+}, increasing Fe-O bond length increases the isomer shift on the tetrahedral sites, and increasing distortion, either by increasing bong length or bond angle variation, results in increasing quadrupole splitting.[49] For 2LFh and 6LFh the electronic densities around Fe^{3+} nuclei are almost identical for Fe1, Fe2 and Fe3 as indicated by almost identical values of the isomer shift. The symmetry around iron nuclei on O_h sites Fe1 and Fe2 with absolute values $|\Delta E_Q| \approx 0.04 – 0.08$ mm/s could however be slightly more distorted than for the T_d sites Fe3 with $|\Delta E_Q| \approx 0.01 – 0.02$ mm/s probably due to slightly different Fe-O bond angle variation.

4 Conclusions

Structural and magnetic properties of 2- and 6-line Fh samples prepared by rapid hydrolysis of $Fe(NO_3)_3 \cdot 9H_2O$ solutions are discussed. Fe *L*-edge EELS results provide evidence of the presence of Fe^{3+} on T_d sites for both the 2- and 6-line Fh samples in agreement with the model proposed by Michel and co-workers. Better NLLS fits for Fh L_3 edges were obtained using reference iron standards with known coordination environment and the percentage of Fe^{3+} in T_d coordination was estimated. The significant amount of tetrahedrally coordinated Fe^{3+} obtained from EELS analysis of 2LFh and 6LFh are consistent with those predicted from Michel's model.

Both ZFMS and IFMS spectra were also successfully fitted to comply with the model proposed by Michel and co-workers, providing for Fe^{3+} cations in two slightly distorted octahedral sites, Fe1 and Fe3, as well as on tetrahedral sites, Fe3. The relative abundances obtained are from ZFMS and IFMS measurements were also fairly consistent with the relative amounts predicted by Michel's model.

Acknowledgements

The financial support from Sasol technology R&D, the National Research Foundation (NRF), and the Department of Science and Technology (DST) of South Africa is gratefully acknowledged. The research leading to these results has received funding from the European Union Seventh Framework Programme (FP7/2007-2013) under grant agreement No. 312483 (ESTEEM2). The corresponding author would also like to acknowledge Dr Andy Brown and Dr Gareth Vaughan from the University of Leeds and superSTEM, respectively for assisting him with the use of IGOR software for EELS data fitting and useful discussions.

References

1. V.A. Drits, B.A. Sakharov, A.L. Salyn, and A. Manceau, Clay Miner., 1993, **28**, 185-207.
2. F.M. Michel, L. Ehm, S.M. Antao, P.L. Lee, P.J. Chupas, G. Liu, D.R. Strongin, M.A.A. Schoonen, B.L. Phillips, and J.B. Parise, Sci. Express, 2007, **316**, 1726-1729.
3. A. Manceau, Clay Miner., 2009, **44**, 19-34.
4. D.G. Rancourt and J.F. Meunier, Am. Mineral., 2008, **93**, 1412-1417.
5. F.M. Michel, V. BarrÓn, J. Torrent, M.P. Morales, C.J. Serna, J. Boily, Q. Liu, A. Ambrosini, A.C. Cismasu, and G.E. Brown Jr., PNAS, 2010, **107**, 2787-2792.
6. S.L. Hwang, P.Y. Shen, H.T. Chu, and T.F. Yui, Int. Geol. Rev., 2006, **48**, 754-764.
7. W.H. Casey, Chem. Rev., 2006, **106**, 1-16.
8. L. Cavé, T. Al, D. Loomer, S. Cogswell, and L. Weaver, Micron, 2006, **37**, 301-309.

9. S.-H. Chen, A. Gloter, A. Zobelli, L. Wang, C.-H. Chen, and C. Coelliex, Phys. Rev. B, 2009, **79**, 104103.

10. C. Colliex, T. Manoubi, and C. Ortiz, Phys. Rev. B, 1991, **44**, 11402-11411.

11. A. Gloter, M. Zbinden, F. Guyoto, F. Gaill, and C. Colliex, Earth and Planetary Sci. Lett., 2004, **222**, 947-957.

12. R.D. Leapman and L.A. Grunes, Phys. Rev. Lett., 1980, **45**, 397-401.

13. R.D. Leapman, L.A. Grunes, and P.L. Fejes, Phys. Rev. B, 1982, **26**, 614-635.

14. Y. Pan, A. Brown, R. Brydson, A. Warley, A. Li, and J. Powell, Micron, 2006, **37**, 403-411.

15. Y. Pan, K. Sader, J.J. Powell, A. Bletoch, M. Gass, J. Trinick, A. Warley, A. Li, R. Brydson, and A. Brown, J. Struct. Biol., 2009, **166**, 22-31.

16. Y. Pan, G. Vaughan, R. Brydson, A. Bleloch, M. Gass, K. Sader, and A. Brown, Ultramicroscopy, 2010, **110**, 1020-1032.

17. H. Tan, J. Verbeeck, A. Abakumov, and G. van Tendeloo, Ultramicroscopy, 2012, **116**, 24-33.

18. P.A. van Aken and S. Lauterbach, Phys. Chem. Miner., 2003, **30**, 469-477.

19. P.A. van Aken, B. Liebscher, and V.J. Styrsa, Phys.Chem. Miner., 1998, **25**, 323-327.

20. P.A. van Aken and S. Liebscher, Phys. Chem. Miner., 2002, **29**, 188-200.

21. C. Wang, D.R. Baer, J.E. Amonette, M.H. Engelhard, J. Antony, and Y. Qiang, J. AM. Chem. SOC., 2009, **131**, 8824-8832.

22. A. Manceau and W. Gates, Clay Clay Miner., 1997, **45**, 448-460.

23. D.B. Williams and C.B. Carter, *Transmission Electron Microscopy*, Springer Science+Bussness Media, LLC, New York, 2009.

24. B. Douglas, D. McDaniel, and J. Alexander, *Concepts and Models of Inorganic Chemistry*, John wiley & Sons, Inc., New York, 1994.

25. D. Peak and T. Reiger, Environ. Sci. Technol. , 2012, **46**, 3163-3168.

26. Y. Pan, Ph.D Thesis, University of Leeds, 2007.

27. T.R. D. Peak, Environ. Sci. Technol. , 2012, **46**, 3163-3168.

28. Y. Guyodo, P. Sainctavit, M. Arrio, C. Carvallo, R.L. Penn, J.J. Erbs, B.S. Forsberg, G. Morin, F. Maillot, F. Lagrox, P. Bonville, F. Wilhelm, and A. Rogalev, Geochem. Geophys. Geosyst., 2012, **13**, 1-9.

29. S. Bali, G. Bali, F.E. Huggins, M.S. Seehra, V. Singh, J.M. Hancock, R. Harrison, G.P. Huffman, R.J. Pumire, R.D. Ernest, and E.M. Eyring, Ind. Eng. Chem. Res. , 2012, **51**, 4515-4522.

30. U. Schwertmann and R.M. Cornell, *Iron Oxides in the Laboratory*, Wiley-VCH, New York, Second, Completely, Revised, and Extended ed, 2000.

31. D. Carta, M.F. Casula, A. Corrias, A. Falqui, G. Navarrra, and G. Pinna, Mater. Chem. Phys., 2009, **113**, 349-355.

32. C.J. Masina, J.H. Neethling, E.J. Olivier, E. Ferg, S. Manzini, L. Lodya, P. Mohlala, and M.W. Ngobeni, Thermochim. Acta, 2015, **599**, 73-83.

33. R.L. Espinoza, A.P. Steynberg, B. Jager, and A.C. Vosloo, Appl. Catal. A: General, 1999, **186**, 13-26.

34. C.T. Koch, W. Sigie, R. Höschen, M. Rütle, E. E., G. Benner, and M. Matijevic, Microsc. Microanal., 2006, **12**, 506-514.

35. R.F. Egerton, *Electron Energy-Loss Spectroscopy in the Electron Microscope*, Springer Science + Business Media, LLC, New York, 2nd ed, 2011.

36. R.M. Cornell and U. Schwertmann, *The iron oxides: Structure properties, reactions, occurrences, and uses*, Wiley-VCH Verlag GmbH & CO, Weinheim, Second, completely revised and extended ed, 2003.

37. F. Maillot, G. Morin, Y. Wang, D. Bonnin, P. Ildefonse, C. Chaneac, and G. Calas, J. Geochim. Cosmochim. Acta, 2011, **75**, 2708-2720.

38. A.B. Y. Pan, R. Brydson, A. Warley, A. Li, J. Powell, Micron, 2006, **37**, 403-411.

39. J.P. Crocombette, M. Pollak, F. Jollet, N. Thromat, and M. Gautier-soyer, Phys. Rev., 1995, **52**, 3143-3150.

40. A. Manceau, Environ. Sci. Technol., 2012, **46**, 6882-6884.

41. D. Peak and T. Reiger, Environ. Sci. Technol., 2012, **46**, 6885-6887.

42. E. Murad and J. Cashion*, Mössbauer spectroscopy of Enviromental Materials and their Industrial Utilization,* Kluwer Acadamic Press, Boston, 2004.

43. D.B. Hausner, N. Bhadari, A. Pierre-Louis, J.D. Kubicki, and D.R. Strongin, J. Colloid Interface Sci., 2009, **337**, 492-500.

44. Y. Guyodo, S.K. Banerjee, R.L.B. Penn, D., T.S. Berquo, T. Seda, and P. Solheid, Phys. Earth Planet. In., 2006, **154**, 222-233.

45. E. Murad and U. Schwertmann, Am. Mineral., 1980, **65**, 1044-1049.

46. Q.A. Pankhurst and R.J. Pollard, Clay Clay Miner., 1992, **40**, 268-272.

47. J. Zhao, F.E. Huggins, Z. Feng, and G.P. Huffman, Clay Clay Miner., 1994, **42**, 737-746.

48. E. Murad, J. Magn. Magn. Mater., 1988, **74**, 153-157.

49. C.M. Cardile and I.W.M. Brown, Clay Miner., 1988, **23**, 13-25.

50. C.W. Childs and J.H. Johnston, Aust. J. Soil Res., 1980, **18**, 245-250.

51. A.G. Maddock, *Mössbauer Spectroscopy: Principles and Applications*, Horwood Publishing, Chichester, 1997.

52. M.B. Madsen, S. MØrup, and C.J.W. Kock, Hyperfine Interact., 1986, **27**, 329-332.

53. E. Murad and F.N.J. Weihenstephan, Miner. Mh., 1982, **H.2**, 45-56.

54. W. Chen, S. Mørup, M.F. Hansen, T. Bnet, and U.A. Peuker, J. Magn. Magn. Mater., 2008, **320**, 2099-2105.

55. S. Linderoth, P.V. Hendriksen, F. Bødker, S. Wells, K. Davies, S.W. Charles, and S. Mørup, J. Appl. Phys., 1994, **75**, 6583-6585.

Figure captions

Figure 1: Fe $L_{2,3}$ edges of 2LFh, 6LFh and different Fe oxide reference materials. The Fe $L_{2,3}$ spectra are vertically shifted for clarity.

Figure 2: NLLS fit of 2LFh showing the mismatch at the lower energy side of the main Fe $L3$ peak. The spectrum was fitted with a hematite and maghemite reference spectra. The difference spectrum is plotted on the same scale, however shifted vertically for clarification.

Figure 3: EELS spectrum of 2LFh spectrum (black) and calculated fit curve (red), and the relative content of reference materials that produced the best NLLS fit. The difference spectrum is plotted on the same scale, however shifted vertically for clarification.

Figure 4: The EELS spectrum of 6LFh (black) and corresponding best fit curve (red), and the relative proportions of the three reference compounds that produced the best NLLS. The difference spectrum is plotted on the same scale, however shifted vertically for clarification.

Figure 5: Mössbauer spectra recorded at 4.2 K for (a) 2LFh and (b) 6LFh. Fe1, Fe2 and Fe3 correspond to the three types of Fe sites in ferrihydrite structure, i.e. octahedrally (Fe1 and Fe2) and tetrahedrally (Fe3) coordinated sites.

Figure 6: Mössbauer spectra recorded at 4.2 K in an applied magnetic field of 10 T parallel to the direction of γ-rays for (a) 2LFh and (b) 6LFh. Fe1, Fe2 and Fe3 correspond to the three types of Fe sites in ferrihydrite structure, i.e. octahedral (Fe1 and Fe2) and tetrahedral (Fe3).

Table captions

Table 1: Fitting coefficients for 2LFh and 6LFh from NLLS fitting without and including wüstite in the fitting routine. χ^2 is calculated following equation (1).

Table 2: Mössbauer parameters of 2LFh and 6LFh obtained from the spectra recorded at 4.2 K and at 4.2 K in an applied magnetic field of 10 T parallel to the direction of γ-rays.

Figures

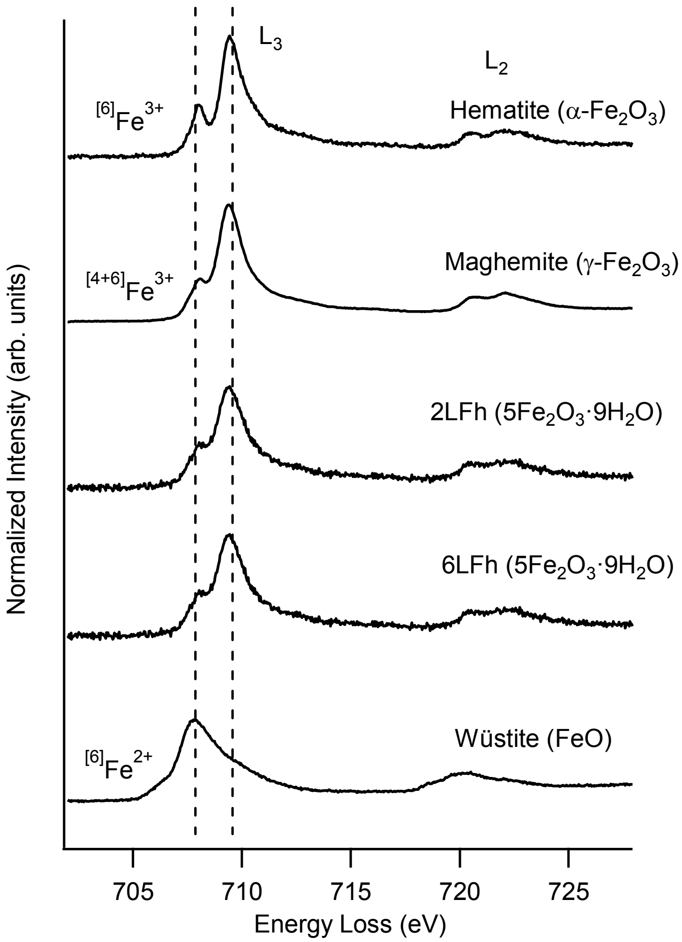

Figure 1:

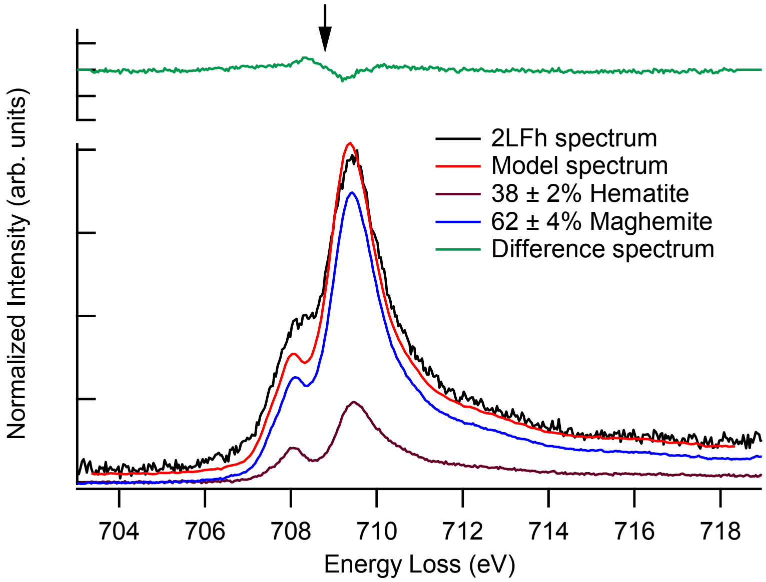

Figure 2:

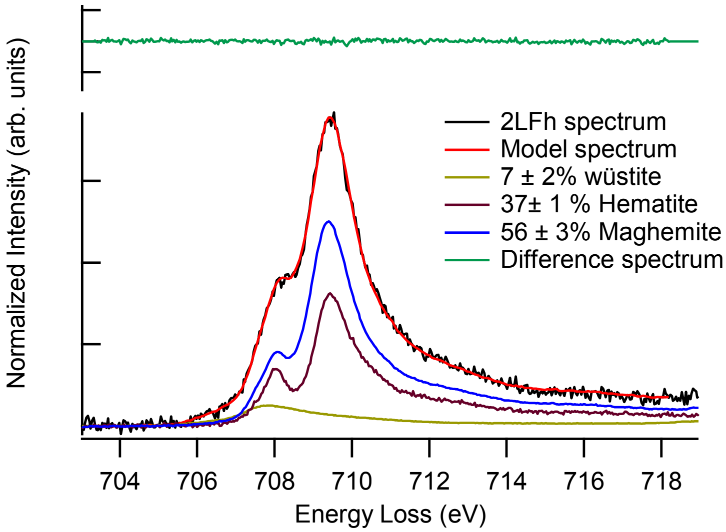

Figure 3:

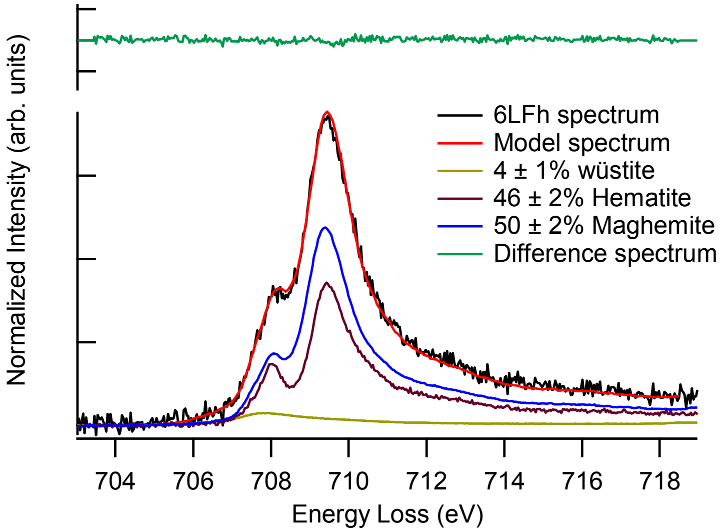

Figure 4:

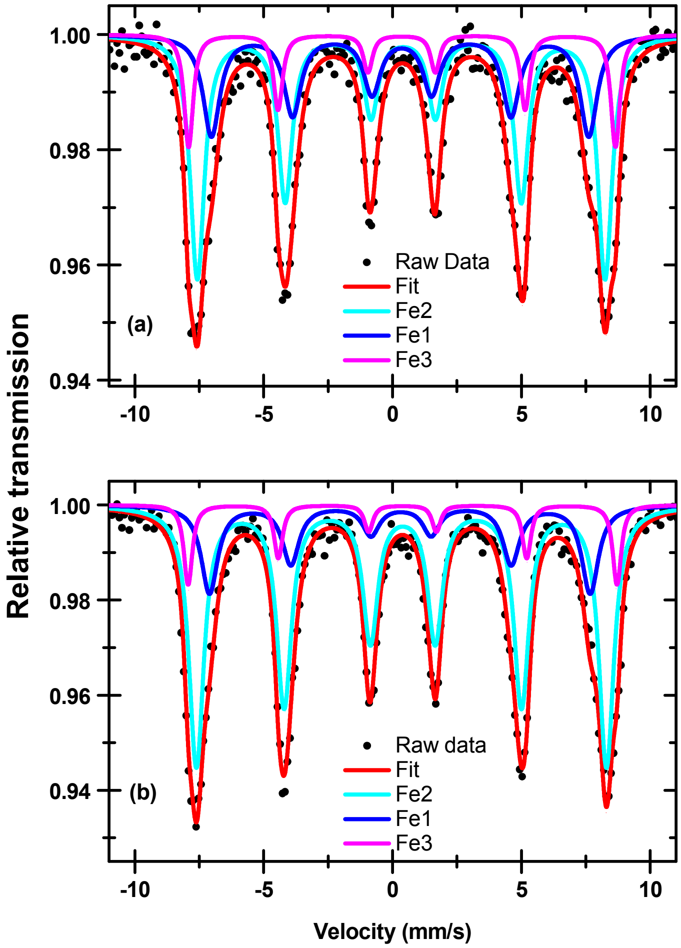
Relative transmission
1.00
0.98
0.96
0.94
-10
-5
0
5
10
(a)
Raw Data
Fit
Fe2
Fe1
Fe3
1.00
0.98
0.96
0.94
(b)
Raw data
Fit
Fe2
Fe1
Fe3
-10
-5
0
5
10
Velocity (mm/s)

Figure 5:

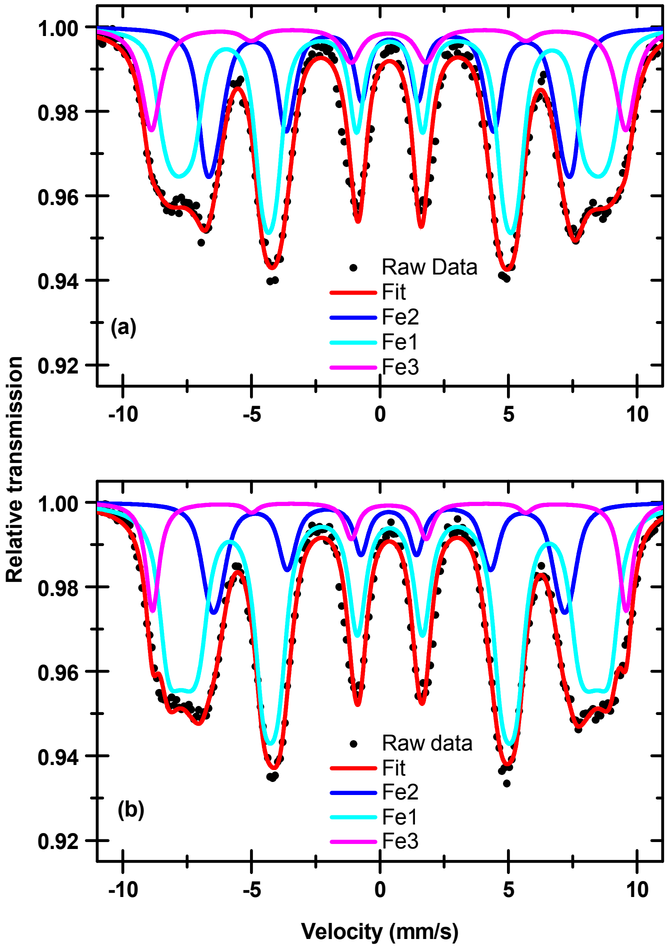
1.00
0.98
0.96
0.94
0.92
(a)
Raw Data
Fit
Fe2
Fe1
Fe3
-10
-5
0
5
10
Relative transmission
(b)
Raw data
Fit
Fe2
Fe1
Fe3
Velocity (mm/s)

Figure 6:

Tables

Table 1:

Sample	Fitting Coefficients ($\sum = 1$)			χ^2
Reference	α-Fe_2O_3	γ-Fe_2O_3	FeO	
2LFh	0.38 ± 0.0082	0.62 ± 0.0232	-	2.53×10^{-5}
	0.37 ± 0.0027	0.56 ± 0.0157	0.07 ± 0.0016	6.00×10^{-6}
6LFh	0.40 ± 0.0071	0.60 ± 0.0170	-	1.56×10^{-5}
	0.46 ± 0.0093	0.50 ± 0.0120	0.04 ± 0.0005	7.13×10^{-6}

Table 2:

Sample	T (K)	B_{app} (T)	$^{\#}\delta$ (mm/s)	$^{\#}\Delta$ (mm/s)	B_{hf} or B_{eff} (T)	▪A (%)	Fe sites
2LFh	4.2	0	0.49	-0.08	49.1 ± 0.6*	53	Fe1 O_h
			0.44	-0.07	45.4 ± 0.2*	31	Fe2 O_h
			0.47	0.02	51.4 ± 0.2*	15	Fe3 T_d
	4.2	10	0.47	-0.04	50.4 ± 2.9**	54	Fe1 O_h
			0.48	-0.02	43.2 ± 1.7**	30	Fe2 O_h
			0.45	0.04	57.2 ± 0.8**	16	Fe3 T_d
6LFh	4.2	0	0.50	-0.05	49.3 ± 0.1*	67	Fe1 O_h
			0.43	-0.07	45.5 ± 0.1*	23	Fe2 O_h
			0.50	0.01	51.6 ± 0.1*	10	Fe3 T_d
	4.2	10	0.48	-0.04	49.7 ± 3.1**	69	Fe1 O_h
			0.47	-0.04	42.3 ± 1.6**	20	Fe2 O_h
			0.47	0.02	57.1 ± 0.6**	11	Fe3 T_d

(*): Hyperfine magnetic field, B_{hf}

(**): Effective magnetic field, B_{eff}, measured in an applied magnetic field of 10 T

Uncertainties: $^{\#}$ ± 0.02 mms^{-1}, ▪ ± 2%, the uncertainties on B_{eff} are the standard deviations of the distributions of B_{eff}.